Available online at www.sciencedirect.com
SCIENCE DIRECT®
Sensors and Actuators A 118 (2005) 49–56
SENSORS AND ACTUATORS A PHYSICAL
www.elsevier.com/locate/sna

Micromachined infrared bolometers on flexible polyimide substrates

Shadi A. Dayeh, Donald P. Butler*, Zeynep Çelik-Butler

Electrical Engineering Department, University of Texas at Arlington, P.O. Box 19072, Arlington, TX 76019, USA

Received 21 April 2004; received in revised form 28 July 2004; accepted 29 July 2004
Available online 11 September 2004

Abstract

Micromachined infrared sensor arrays have been fabricated on flexible polyimide substrates using a silicon wafer carrier during the fabrication process. These flexible polyimide substrates containing the micromachined infrared sensors were removed from the silicon wafer at the end of fabrication. The fabrication technique utilized surface micromachining of a bridge structure to form the thermal infrared (IR) sensors on flexible substrates. Semiconducting yttrium barium copper oxide YBCO was used as the radiation sensitive material. 1×10 sensor arrays of microbolometers were micromachined using a photo-definable polyimide sacrificial layer and characterized before and after removal of the substrate from the Si wafer carrier. The flexible infrared microsensors showed similar performance to microbolometers fabricated on rigid silicon substrates. The YBCO thermistors exhibited a temperature coefficient of resistance (TCR) of $\sim -3.4\%\ K^{-1}$ near room temperature. Responsivity and detectivity values as high as 6.1×10^4 V/W and 1.2×10^8 cm $Hz^{1/2}$/W, respectively, were measured in vacuum for a 40 μm $\times$ 40 μm microbolometer with 1 μA bias. The lowest observed noise equivalent power was 4.1×10^{-11} W/$Hz^{1/2}$ while the lowest thermal time constant was 5.7 ms.

Keywords: Microbolometers; Flexible substrate; micromachining; Yttrium barium copper oxide; MEMS; Smart skin

1. Introduction

Microelectromechanical systems (MEMS) are continuously shrinking in size to reduce mass, increase resonant frequency and lower the force constants of these systems. Electronic applications are emerging for devices such as displays and sensor arrays on flexible substrates, where it is highly desirable that they be large area, light weight and deformable. In the last two decades, efforts have been made to accomplish a "smart skin" with embedded MEMS sensors that can be applied to non-planar surfaces [1–7]. The properties of these flexible substrates include their light weight, flexibility, potential low cost, and ability to enable applications such as sensitive or smart skin for robotics applications, smart tags and labels, wearable and mobile sensors for military and commercial use. In addition to MEMS, electronic circuitry has also been implemented on flexible substrates. Transistors on thin metal or plastic foil substrates and polyimide films have been demonstrated [8–11]. Semiconductor electronics and MEMS sensors are envisioned to merge, forming a flexible smart skin that mimics the sensory perception of human skin.

Some of the current flexible electronic technology utilizes devices fabricated on plastic substrates by thin film deposition to form heat flux [7] and thermal infrared (IR) sensors [12]. In other cases, devices are fabricated on polymer and polyester substrates [2–6]. On polyimide substrates, silicon islands connected by polyimide films have been used to achieve a flexible pressure sensor technology. Si-diode temperature sensors [2,5] and shear stress sensors [4] have been demonstrated. A tactile sensor based on polymer micromachining techniques applied to the Si wafer carrier has also been reported [1]. In this case, the polyimide layer was released from the surface-treated-Si wafer using a buffered hydrofluoric acid at the end of the fabrication. This is similar to

* Corresponding author. Tel.: +1 817 272 1305; fax: +1 817 272 7458.
E-mail address: dbutler@uta.edu (D.P. Butler).

0924-4247/$ – see front matter © 2004 Elsevier B.V. All rights reserved.
doi:10.1016/j.sna.2004.07.009

our work [13]. However, our flexible sensor arrays required micromachining of the microbolometer structure on the flexible polyimide substrate as described later.

Microbolometers on rigid Si substrates represent a relatively mature technology, utilizing several materials as the thermometer such as VO_x [14,15], poly-Si–Ge [16,17], YBCO [18], or metal resistors such as, titanium [19], and niobium [20]. Bulk micromachined $Ge_xSi_{1-x}O_y$ sensors have shown a large temperature coefficient of resistance (TCR) of $-4.2\%\,K^{-1}$ at room temperature, exhibiting a responsivity of 380 V/W at 100 nA of current biasing [21]. Surface micromachined detectors using polyimide sacrificial layers and amorphous silicon (a-Si) thermistors were demonstrated with a TCR of $-2.5\%\,K^{-1}$ and a thermal conductance of 8.3×10^{-8} W/K using thin TiN electrode arms, and a responsivity of 10 mV/K [22]. This works seeks to extend the research on micromachined bolometers on rigid substrates to flexible substrates. By utilizing a flexible substrate, an infrared detector array can conform to a non-planar surface, provided that the required optical components can be incorporated to the sensor at the device level.

Previous work on IR detectors on flexible substrates used Kapton sheets bonded to Si wafers. At the end of the fabrication, the Kapton sheets were removed from the silicon wafer carriers. These sensors achieved a responsivity of 2×10^3 V/W and a detectivity of 3×10^7 cm $Hz^{1/2}$/W at 1 μA of current even though the sensors maintained full thermal contact with the substrate [12]. However, two problems were faced while working on Kapton sheets: misalignment and yield. Due to trapped air bubbles while bonding the Kapton sheets to silicon and because of the thermal expansion of the Kapton film during fabrication, misalignment to the photolithographic masks was a problem that resulted in lower yield. Later, detectors that utilized spin-cast polyimide films as the flexible substrate were investigated [23]. No noticeable problems were found during fabrication on polyimide films, but the films were not separated from the silicon wafer to achieve the desired flexibility. These sensors achieved a responsivity of 3.5×10^3 V/W and a detectivity of 9.9×10^6 cm $Hz^{1/2}$/W at 2.88 μA of current. These sensors were also not micromachined.

In this work, the performance of the infrared microbolometers has been improved by micromachining a bridge structure under the thermistor. As a result, the thermal conductance between the microbolometer and the substrate was decreased resulting in a higher responsivity. The polyimide containing the sensors was then removed from the silicon wafer and the sensors were tested when curved. The flexible substrate used in this work was a spin-cast PI-5878G, an HD Microsystems high temperature polyimide coating [24]. PI-5878G was thermally converted into intractable polyimide film after it was applied to the silicon substrate. PI-5878G has a glass transition temperature (T_g) of 400 °C. Thus, it requires low-temperature processing when compared to devices on silicon substrates but it is flexible and has a great potential for low cost and large area electronics.

2. Infrared detection

A wide variety of civilian and military applications employ infrared sensors [25]. Two types of IR sensors are being used: (1) photon sensors where incident photons create electron–hole pairs; (2) thermal sensors where radiation changes the temperature of the sensor thereby modifying the electrical characteristics of the sensitive material. A bolometer is a thermal sensor whose resistance value changes with incident radiation. Taking into consideration the thermodynamic interactions between the microbolometer and its surroundings, the following heat transfer equation can be derived, neglecting the radiative conductance [26]:

$$C_{\text{th}}\frac{\mathrm{d}\,\Delta T}{\mathrm{d}t} + (G_{\text{th}} - \alpha_0 P_I)\,\Delta T = \eta P + P_I \tag{1}$$

where C_{th} is the thermal capacity of the microbolometer, ΔT is the incremental temperature change of the microbolometer, G_{th} is thermal conductance from the microbolometer to the substrate, α_0 is the TCR ($\alpha_0 = (1/R)(\mathrm{d}R/\mathrm{d}T)$), P_I is the heating power due to the bias current, η is the absorptivity of the thermometer, and P is the incident light flux.

The modulated output voltage when divided by the input light flux results in a voltage responsivity in the form of:

$$R_v = \frac{\eta\alpha_0 R I_b}{G_{\text{eff}}(1+\omega^2\tau_{\text{eff}}^2)^{1/2}} = \frac{\kappa\alpha_0 I_b R}{\sqrt{1+\omega^2\tau_{\text{eff}}^2}} \tag{2}$$

where G_{eff} is the effective thermal conductance ($G_{\text{eff}} = (G_{\text{th}} - \alpha_0 P_I)$), τ_{eff} is the effective thermal time constant ($\tau_{\text{eff}} = (C_{\text{th}}/(G_{\text{th}} - \alpha_0 P_I)) = (C_{\text{th}}/G_{\text{eff}})$), and κ is the thermodynamic efficiency ($\kappa = (\eta/(G_{\text{th}} - \alpha_0 P_I))$). The effect of the bias current heating power on the voltage responsivity in Eq. (2) is seen in Fig. 1. These effects are strong in the case of low thermal conductance values where the bias power is no

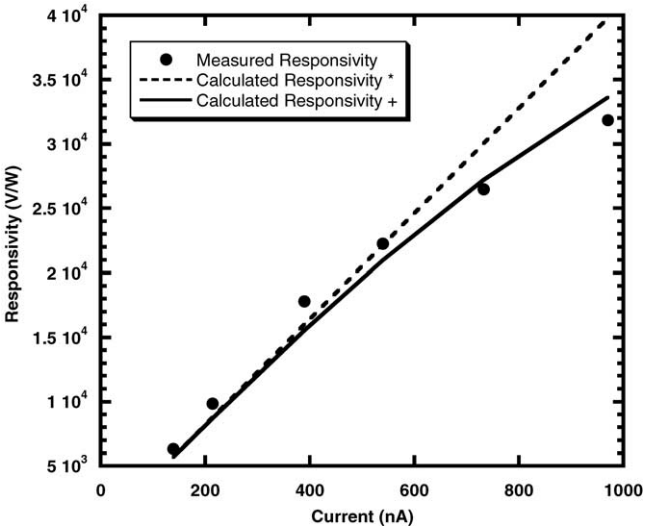

Fig. 1. Comparison of responsivity calculations with (+) and without (*) biasing current effects to the measured responsivity at room temperature for device DD10 (see Table 1 for device description).

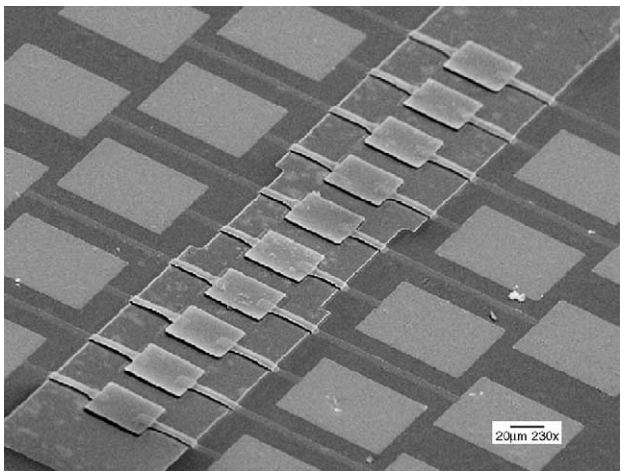

Fig. 2. A SEM micrograph of a 1 × 10 array consisting of 60 μm × 60 μm microbolometers.

longer negligible when compared to the thermal conductance, which is the case for the current microbolometers. Other bolometers figures of merit are extensively dealt with and can be found elsewhere [25,26]. The infrared microbolometers reported in this paper include 40 μm × 40 μm and 60 μm × 60 μm geometries in a 1 × 10 array configuration. A SEM micrograph of the 60 μm × 60 μm 1 × 10 array is shown in Fig. 2. The micrograph (Au coated) was taken after micromachining the bolometers.

3. Microbolometer fabrication

Infrared microbolometers fabricated on polyimides require more attention to the processing temperature than those fabricated on rigid silicon. Polyimide layers were applied to the silicon wafer after being coated with a 400 nm Si_3N_4 layer. All material depositions (other than polyimides) were performed by a rf magnetron sputtering system in a 10 mTorr Ar environment. Five layers of PI-5878G were spin-coated on the Si wafer to form the flexible polyimide substrate and removed from the carrier wafer at the end of fabrication. To achieve greater uniformity of the polyimide film, spin coating started at 2000 rpm and was increased 100 rpm for each successive layer. After the soft bake at 110 °C for 6 min, the polyimide film (∼40-μm thick) was cured for five hours in an oven at 275 °C in air environment. To passivate the polyimide film and to enhance the adhesion to the subsequent device layers, a 400 nm Si_3N_4 layer was sputtered at 200 W. Aluminum does not adhere properly to the polyimide layer, which agrees with [3]. The nitride intermediate layer also withstands most of the chemical wet etchants used in our fabrication process and results in good adhesion between the polyimide film and the subsequent microbolometer layers. Si thin film transistors on plastic substrates also often use a silicon nitride or silicon dioxide buffer layer between the plastic substrate and the silicon layer, thus compatibility with the integration with electronics is achieved.

Next, a 70 nm $SrTiO_3$ dry etch stop was sputtered above the nitride layer (Fig. 3a). To form a micro-mirror that reflects the radiation directly under the pixel, a 260-nm thick Al layer was sputtered and subsequently patterned in square geometries of the same area as the YBCO thermometer (Fig. 3b).

A sacrificial layer was used to form the bridge structure and was removed at the end of the fabrication. A 1.9 μm PI2737 photo-definable polyimide sacrificial layer was spin-coated at 2900 rpm and soft baked at 65 °C and 95 °C sequentially, 1 min each. After patterning the sacrificial layer, extending 50 μm around the pixel, the metallization layers were deposited (Fig. 3c). A combination of Ti electrode arms and Au contacts/bonding pads was used. Ti has a low thermal conductance of 0.219 W/cm K. Using Ti as electrode arms, the energy transfer from the YBCO thermometer to the substrate can be minimized, thus increasing responsivity. Ti electrode arms were patterned by lift-off using a 1.5-μm thick negative photoresist. A 100 nm Ti layer was sputtered to form the electrode arms between the YBCO thermometer and the bond pads, followed by a 70-nm thick film of Au to form the bond pads and electrical contacts to the YBCO thermistor. Then, lift-off was performed to define both the Ti and Au layers. The portion of Au extending beyond the bond pads and the contacts was etched in a KI:I_2 solution (Fig. 3d). A composite $YBa_2Cu_3O_{6+x}$ target was used to sputter the 400-nm thick YBCO layer. YBCO exhibits a high measured TCR value of $-3.4\%\,K^{-1}$ at room temperature without the need for substrate heating during deposition or post-deposition thermal annealing. A diluted Al-etch solution was used to pattern the YBCO pixels (Fig. 3e). The sensor was formed after this step and the wafer was divided into six pieces. The sacrificial layer (PI2737) in some of the pieces was removed by O_2 plasma ashing to suspend the microbolometers, which we refer to as micromachined bolometers (Fig. 3f). Other microbolometers, with the sacrificial layer in place, which we refer to as non-micromachined bolometers, were also tested.

To separate the polyimide film from the silicon wafer, a sharp knife was used at the corners of four-die pieces. These pieces were individually immersed for short time in deionized water until the polyimide layer was separated from the underlying nitride layer on the silicon wafer. This might be explained with the fact that the nitride layer is hydrophobic whereas the polyimide layer, formed from polyamic acid, contains many OH and NH groups, and thus hydrophilic [24]; No strong H-bonds are present between the two layers, and DI H_2O diffuses easily to separate them. The detached films were blown with N_2 to dry afterwards. Thus, the polyimide substrate was separated from the silicon wafer carrier to produce IR microsensors on a flexible substrate (Fig. 4).

4. Experimental results and discussion

Single *dies* were packaged and wire-bonded. The die was mounted to the package by heated solder in some cases where the die deforms and sticks to the solder when cooled to room

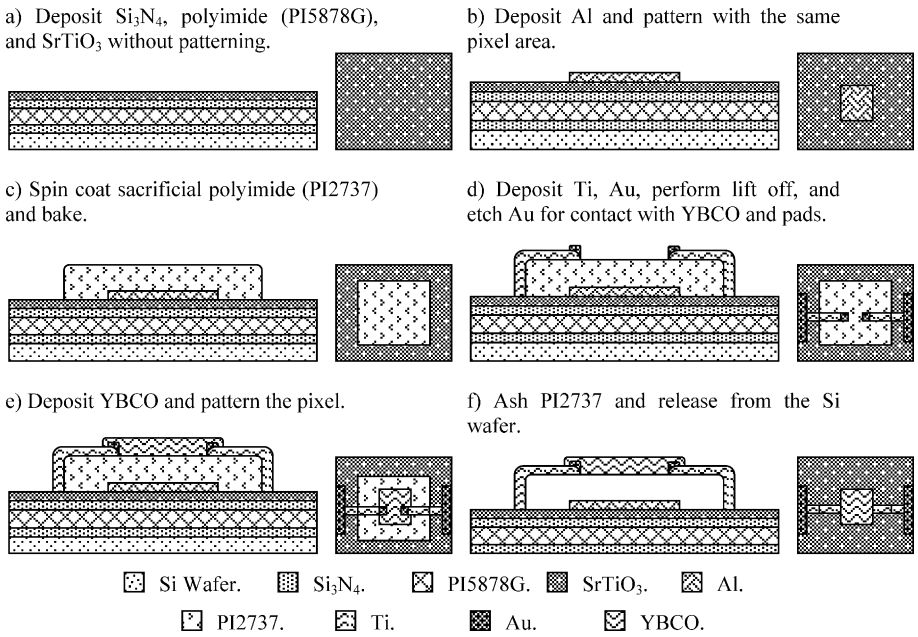

Fig. 3. Schematic diagram for the fabrication process steps in a side view (left) and top view (right) of a single microbolometer on flexible substrate (not drawn to scale).

temperature (DD12, DD15). Others were mounted to the substrate with commercial glue (DD28). However, the curling of the polyimide films during the packaging process made the packaging/bonding process challenging. We have used an ultrasonic wire bonder to wire these devices. The soft polymer tended to absorb the ultrasonic energy and deform with the compressive pressure of the needle making the wire bonding challenging, especially for the curved devices. Failure was encountered due to the breakage of the wire bonds because of the vibrations and because of the relatively high thermal coefficient of expansion of the polyimide (20 ppm for 10 μm film [24]). This problem was encountered also in [27]. In this case, a hard base layer (sulfamate nickel) was deposited above the metal lines (Au,Cu) to facilitate wire bonding with the use of a ball bonder. Others investigating flexible substrates had packaged their devices by flip–chip bonding and mounted rigidly to copper-clad printed circuit board (PCB) [1]. As a consequence of the bond failures, a complete characterization of some of the devices was not possible. This underscores the need for device-level packaging of the flexible detectors.

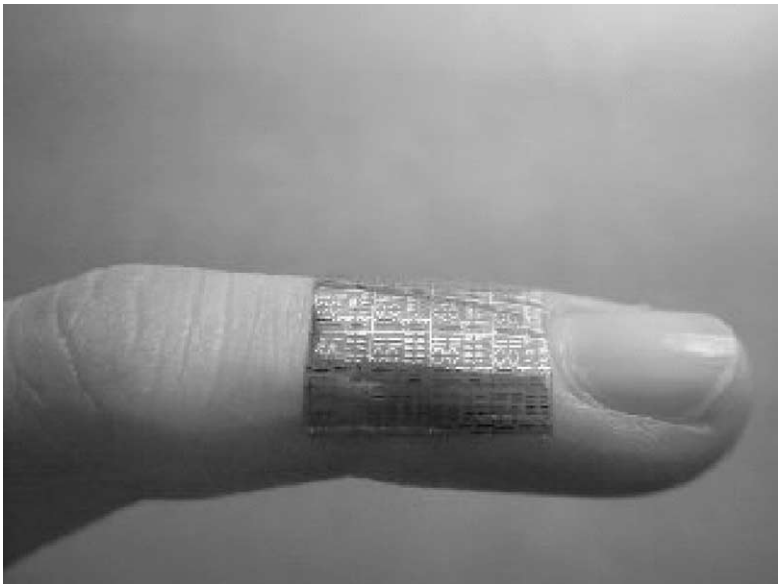

Fig. 4. A flexible “skin” applied to a finger.

The performance of the micromachined and non-micromachined IR microsensors was measured, before and after separation of the polyimide substrate from the silicon wafer carrier. Table 1 summarizes the performance of the tested microbolometers.

The packaged devices were mounted in a Leybold ROK 10–300 K closed-cycle refrigerator evacuated to ∼100 mTorr to measure their resistance (*R–T*) characteristics and determine the TCR. Device DD10 is a micromachined bolometer on a flexible substrate that was not separated from the silicon wafer. The resistance of DD10 decreased exponentially from 70.5 MΩ at 220 K to 1.4 MΩ at 310 K, while the TCR increased from $-5.47\%\,K^{-1}$ at 220 K to $-2.9\%\,K^{-1}$ at 310 K. The *I–V* characteristics were measured at a constant temperature through an HP4142 dc source/monitor unit with current ranging between −2 and 2 μA. The thermal conductance *G* was calculated from the current–voltage (*I–V*) characteristics by Joule heating method. The resistance of the microbolometer at each current value was calculated from the *I–V* measurements, and was plotted versus dissipated power. The slope of this plot was used to calculate the thermal conductance according to the following relation:

$$R(T) = R_0 + \frac{1}{G}\frac{dR}{dT} I_b^2 R(T) \quad (3)$$

The thermal conductance of DD10 was 4.0×10^{-7} W/K at 290 K. A non-micromachined device (DD1) from an adjacent die showed a *G* of 9.1×10^{-6} W/K. This difference in the thermal conductance is a result of the thermal isolation achieved due to removal of the sacrificial layer under the microbolometer. In vacuum, low thermal conductance values can be achieved resulting in high responsivity detectors. The lowest *G* attained in earlier generation, non-micromachined IR sensors with the same device geometry on flexible substrates was 4.2×10^{-5} W/K for Kapton substrates [12], and 3.4×10^{-5} W/K for spin-cast polyimide substrates [23].

Fig. 5 shows the *I–V* characteristics, the *R–T* and the TCR measurements for DD10. As the current bias is increased, the dissipated power in the microbolometer increases, resulting in the non-linear *I–V* curve shown in Fig. 5. Devices with higher thermal conductance (DD7, a micromachined device not separated from silicon with $G = 7.8 \times 10^{-7}$ W/K) attained more linear *I–V* characteristics than DD10.

Device DD15 is a micromachined bolometer on a flexible substrate separated from silicon. The response of DD15 for light modulation at 32 Hz and 1 μA bias current is shown in Fig. 6a. For all microbolometers, optical characteristics were determined through illumination with broadband radiation from an Infrared Industries (manufacturer) thermal blackbody source whose temperature is controlled by a model 101C temperature controller. Throughout the measurements, the temperature of the source was kept at 990 °C and the measurements were performed in air and in vacuum through a ZnSe window. A chopper was used to modulate the IR radiation. The bolometer was biased from a battery-powered low-noise current source with different current values rang-

Table 1
Characteristics of the tested microbolometers on the polyimide substrates

	DD1	DD6	DD10	DD12	DD13	DD15	DD28	DD31	DD33
Microbolometer area (cm^2)	36×10^{-6}	16×10^{-6}	16×10^{-6}	16×10^{-6}	16×10^{-6}	16×10^{-6}	16×10^{-6}	16×10^{-6}	16×10^{-6}
Micromachined	No	Yes	Yes	No	No	Yes	Yes	Yes	Yes
separated from Si	No	No	No	Yes	Yes	Yes	No	Yes	No
Resistance (MΩ) at 290 K	12.6	3.8	3.29	8.24	3.4	3.11	3.5	5	4.89
%TCR(K^{-1}) at 290 K	−3.2	–	−3.4	−3.43	–	–	–	–	–
G_{th} (W/K) at 290 K	9.1×10^{-6}	–	4×10^{-7}	3.3×10^{-6}	–	–		–	–
Measured responsivity (V/W), at 1 μA and 11 Hz	–	3.2×10^4	3.9×10^4	1.1×10^4	4.7×10^3	6.1×10^4	1.9×10^4	2.55×10^4	2.87×10^4
Measured detectivity (cm $Hz^{1/2}$/W), at 1 μA and 11 Hz	–	4.2×10^7	1.1×10^8	9.23×10^6	1.8×10^7	1.2×10^8	8.9×10^7	4.2×10^7	1.2×10^7
Thermal time constant τ_{th} (ms)	–	7.09	5.68	–	–	6.0	–	–	–
Thermal capacitance *C* (J/K)	–	–	2.4×10^{-9}	–	–	–	–	–	–
Absorption coefficient, η	–	–	0.29	–		–	–	–	–
NEP(W/$Hz^{1/2}$)	–	1.7×10^{-10}	4.1×10^{-11}	6.7×10^{-10}	1.0×10^{-9}	4.09×10^{-11}	5×10^{-11}	8×10^{-11}	4.6×10^{-10}

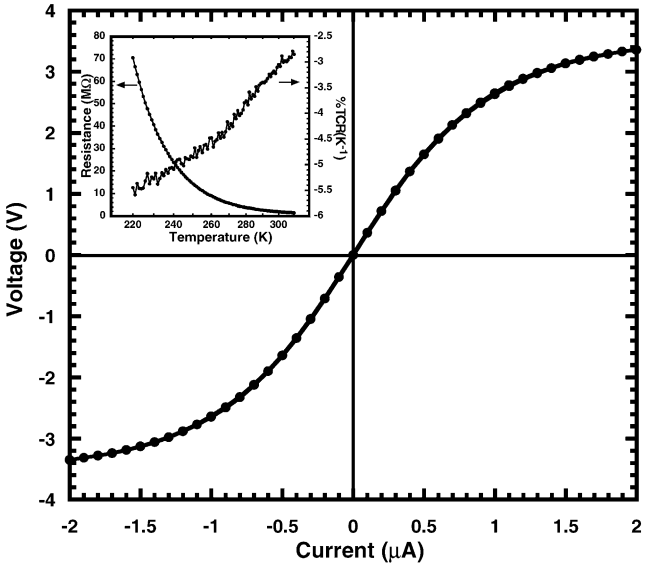

Fig. 5. Current–voltage characteristics of DD10 at room temperature. Resistance vs. temperature and temperature coefficient of resistance measurements are also shown in the inset.

ing from 0.139 to 2.88 μA. The vacuum measurements were performed at ∼70 mTorr inside a cryostat. The output voltage was amplified by a PAR113 low-noise pre-amplifier and was measured by an HP 3562A dynamic signal analyzer. The measurements were conducted in a low-frequency shielded room. Fig. 6b shows the voltage responsivity and detectivity for DD15. The detectivity was calculated from the measured responsivity and measured noise spectral density at different frequencies. For low frequencies between 1 and 5.78 Hz, the dc powered chopper has significant voltage fluctuations adding to the system total noise. Thus, the noise power spectral density values used in the detectivity were measured at 32 Hz chopper frequency. The maximum responsivity and detectivity were 6.1×10^4 V/W and 1.2×10^8 cm $Hz^{1/2}$/W, respectively, for DD15 biased at 970 nA. This device has also shown the lowest NEP of 4.1×10^{-11} W/$Hz^{1/2}$ among the detectors tested in this study.

Device DD10 showed a responsivity of 3.9×10^4 V/W and a detectivity of 1.1×10^8 cm $Hz^{1/2}$/W with 1 μA biasing (Fig. 7). The responsivity of DD10 in vacuum (1.4×10^4 V/W) was higher by a factor of 38 over that measured in air (3.6×10^2 V/W) at 11.88 Hz and 0.214 μA current bias. This was a direct result of the low thermal conductance of DD10 due to micromachining. Using the measured thermal conductivity and the thermal time constant observed from the knee-frequency in responsivity, the thermal capacitance C was estimated to be 2.4×10^{-9} J/K, much lower than $C \sim 2.8 \times 10^{-8}$ J/K measured on sensors built directly on spin-cast polyimide [23]. The measured low-frequency R_V, TCR, and G allowed us to estimate η from Eq. (2) to be 29%, an absorptivity higher than the first generation sensors on Kapton ($\eta \sim$ 15–22%) [12] and than the second generation sensors on spin-cast polyimide substrates ($\eta \sim$ 6–9% for bolometers

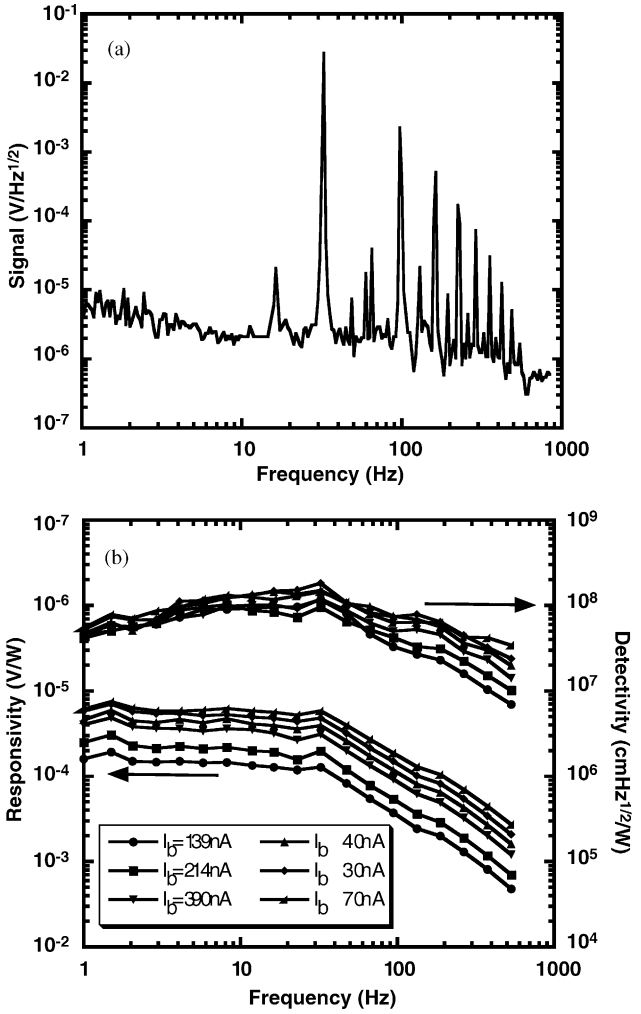

Fig. 6. Optical response of DD15 in vacuum. (a) Output signal power spectral density in response to broad-band incident IR radiation modulated at 32 Hz, with the detector biased at 970 nA. The frequency bandwidth Δf = 0.92 Hz at 32 Hz signal frequency. (b) Measured responsivity and detectivity at different current bias values as a function of radiation modulation frequency.

with no Al reflecting layer ($\eta \sim$ 26 % for bolometers with Al reflecting layer) [23].

Another device DD12 was a non-micromachined bolometer that was separated from the silicon wafer. The maximum responsivity measured from DD12 was 1.1×10^4 V/W and the maximum measured detectivity was 9.23×10^6 cm $Hz^{1/2}$/W. The measured TCR for DD12 was $-3.43\%\ K^{-1}$ at 290 K, similar to that measured on the micromachined sensors (DD10 $-3.4\%\ K^{-1}$ at 290K). However, due to the presence of the polyimide sacrificial layer under the thermometer, the thermal conductance was higher for DD12 ($3.31 \times 10^{-6}\ K^{-1}$) than that of DD10 ($4.0 \times 10^{-7}\ K^{-1}$). Although the resistance of DD12 (8.24 MΩ) was greater than that of DD10 (3.29 MΩ), DD12's maximum responsivity was 1.1×10^4 V/W compared with 3.9×10^4 V/W for DD10. Thus, the response of the non-micromachined sensors was

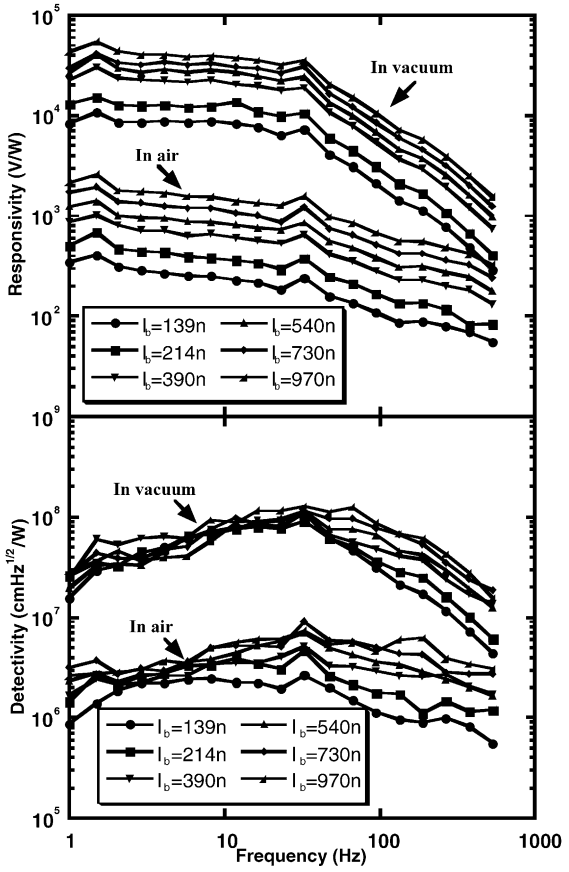

Fig. 7. Responsivity and detectivity measurements on DD10 in vacuum and air vs. radiation modulation frequency.

lower than that of the micromachined sensors. For the micromachined sensors presented in Table 1, the detectors display close values of electrical resistance and responsivity. Nevertheless, the detectivity of DD33 was lower due to the higher noise observed on this device. The characteristics of the microbolometers on polyimide substrates that have been removed from the Si wafer carrier are similar to the microbolometers that have the polyimide substrate still attached to the carrier and to microbolometers fabricated directly on Si in earlier investigations. Sensors described in [18] are structurally similar except they have been fabricated on rigid Si substrates and exhibited a responsivity of $\sim 8 \times 10^3$ V/W and a detectivity of $\sim 1.2 \times 10^8$ cm Hz$^{1/2}$/W at 1 μA of current bias.

Preliminary mechanical tests have shown that bending the flexible substrate over a 1.5 mm radius of curvature did not alter the electrical resistance of most micromachined IR sensors. The effect of bending the substrate to a 1.5 mm radius would provide a minimal effect to typical 40 μm × 40 μm pixels by distorting the pixel about 133 nm. These sensors were damaged, however, when subjected to physical contact. This is to be expected since no superstrate or encapsulation was used in these devices. The flexibility limits of the devices have yet to be fully investigated.

5. Conclusion

1 × 10 micromachined infrared sensor arrays have been demonstrated on flexible polyimide substrates by surface-micromachining polyimide sacrificial layers. The YBCO thermistors were held by thin titanium electrode arms in a bridge structure above the substrate to lower the thermal conductance and achieve high responsivity. The sensors were successfully removed from the silicon wafer carrier and achieved high responsivity and detectivity exceeding 10^4 V/W and 10^8 cm Hz$^{1/2}$/W, respectively. Encapsulating the IR sensors with a polyimide superstrate is currently under investigation. The polyimide superstrate will help in embedding the sensors in a vacuum cavity and will protect them from contact damage. The combination of the superstrate and the substrate will enable encapsulation of the detectors in a low stress plane, minimizing the mechanical strain on the detectors.

Acknowledgements

This work is based in part upon work supported by the NSF under grant ECS-0245612. The authors would like to thank the staff members at the Nanofab Teaching and Research Facility of the University of Texas at Arlington. The authors would like to thank the Cornell Nanofabrication Facility for fabricating the photolithography masks used in this investigation.

References

[1] J. Engel, J. Chen, C. Liu, Development of polyimide flexible tactile sensor skin, J. Micromech. Microeng. 13 (2003) 359–366.
[2] P.W. Barth, S.L. Bernard, J.B. Angell, Flexible circuit and sensor arrays fabricated by monolithic silicon technology, IEEE Trans. Electron Dev. ED-32 (1985) 1202–1205.
[3] D.J. Beebe, D.D. Denton, A flexible polyimide-based package for silicon sensors, Sensors Actuators A44 (1994) 57–64.
[4] Y. Xu, Y. Tai, A. Huang, C. Ho, IC-Integrated flexible shear-stress sensor skin, Solid State Sensor, Actuator and Microsystems Workshop, Hilton Head Island, South Carolina, 2–6 June 2002.
[5] G. Lee, J. Wu, J. Miau, A new fabrication process for a flexible skin with temperature sensor array, J. Chin. Inst. Eng. 25 (2002) 619–625.
[6] N.K.S. Lee, R.S. Goonetilleke, Y.S. Cheung, G.M.Y. So, A flexible encapsulated MEMS pressure sensor system for biomechanical applications, Microsyst. Technol. 7 (2001) 55–62.
[7] C. Bang, T. Pan, Flexible heat flux sensor arrays, AFOSR Contractor and Grantee Meeting on Turbulence and Internal Flows, Atlanta, Georgia, 4–6 September 1996.
[8] E.Y. Ma, S.D. Theiss, M.H. Lu, C.C. Wu, J.C. Sturm, S. Wagner, Thin film transistors for foldable displays, IEEE IEDM Tech. Dig. 1997, 535–538.
[9] H. Gleskova, S. Wagner, Failure resistance of amorphous silicon transistors under extreme in-plane strain, Appl. Phys. Lett. 75 (1999) 3011–3013.
[10] P. Hsu, M. Huang, S. Wagner, Z. Suo, J.C. Sturm, Plastic deformation of thin foil substrates with amorphous silicon islands into

spherical shapes, Mat. Res. Soc. Symp. Proc. 621 (2000) Q8.6.1–Q8.6.6.
[11] Y. Lee, H. Li, S.J. Fonash, High-performance poly-Si TFTs on plastic substrates using a nano-structured separation layer approach, IEEE Electron Dev. Lett. 24 (2003) 19–21.
[12] A. Yaradanakul, D.P. Butler, Z. Çelik-Butler, Uncooled infrared microbolometers on a flexible substrate, IEEE Trans. Electron Dev. ED-49 (2002) 930–933.
[13] S.A. Dayeh, D.P. Butler, Z. Çelik-Butler, P. Wisian-Neilson, Uncooled micromachined bolometer arrays on flexible substrates, SPIE Proc. 5074 (2003) 537–547.
[14] T. White, N. Butler, R. Murphy, An uncooled IR sensor with digital focal plane array, IEEE Eng. Med. Biol. 17 (1998) 60–65.
[15] W. Radford, R. Wyles, J. Wyles, J. Varesi, M. Ray, D. Murphy, A. Kennedy, A. Finch, E. Moody, F. Cheung, R. Coda, S. Baur, Microbolometer uncooled infrared camera with 20 mK NETD, SPIE 3436 (1998) 636.
[16] J. Wauters, Doped silicon creates new bolometer material, Laser Focus World (1997) 145.
[17] S. Sedky, P. Fiorini, K. Baert, L. Hermans, R. Mertens, Characterization and optimization of infrared poly SiGe bolometers, IEEE Trans. Electron Dev. 46 (1999) 675–682.
[18] M. Almasri, D.P. Butler, Z. Çelik-Butler, Self supported uncooled infrared microbolometers with low-thermal mass, J. Microelectromech. Syst. 10 (2001) 469–476.
[19] H.K. Lee, J.B. Yoon, E. Yoon, S.B. Ju, Y.J. Yong, W. Lee, S.G. Kim, A high fill-factor IR bolometer using multi-level electrothermal structures, IEEE IEDM Tech. Digest. (1998) 463–466.
[20] L. Boarino, G. Lerondel, E. Monticone, R. Steni, G. Amato, G. Benedetto, V. Lacquaniti, R. Spagnolo, Design and Fabrication of Metal Bolometers on High Porosity Silicon Layers, 4th THERMINIC Workshop, 27–29 September 1998, Cannes.
[21] E. Iborra, M. Clement, L.V. Herrero, J. Sangrador, IR uncooled bolometers based on amorphous $Ge_xSi_{1-x}O_y$ on silicon micromachined structures, J. Microelectomech. Syst. 11 (2002) 322–329.
[22] J. Tissot, F. Rothan, C. Vedel, M. Vilain, J.-J. Yon, LETI/LIR's uncooled microbolometer development, SPIE Proc. 3436 (1998) 605–610.
[23] A. Yildiz, Z. Çelik-Butler, D.P. Butler, Microbolometers on a flexible substrate for infrared detection, IEEE Sensors J. 4 (2004) 112–117.
[24] HD Microsystems PI-5878G product manual.
[25] E.L. Dereniak, G.D. Boreman, Infrared Detectors and Systems, John Wiley and Sons, 1996.
[26] R.A. Wood, Monolithic silicon microbolometer arrays, in: P.W. Kruse, D.D. Skatrud (Eds.), Uncooled Infrared Imaging Arrays and Systems, Semiconductors and Semimetals, vol. 47, Academic Press, New York, 1997.
[27] E. Hall, A.M. Lyons, J.D. Weld, Gold wire bonding onto flexible polymeric substrates, IEEE Trans. Components, Packag. Manufact. Tech. A19 (1996) 12–17.